c-MET receptor-targeted fluorescence on the road to image-guided surgery in penile squamous cell carcinoma patients

Vries, H.M. de; Bekers, E.; Oosterom, M.N. van; Karakullukcu, M.B.; Poel, H.G. van der; Leeuwen, F.W.B. van; ... ; Brouwer, O.R.

c-MET Receptor–Targeted Fluorescence on the Road to Image-Guided Surgery in Penile Squamous Cell Carcinoma Patients

Hielke M. de Vries[1,2], Elise Bekers[3], Matthias N. van Oosterom[1,2], M. Baris Karakullukcu[4], Henk G. van der Poel[1], Fijs W.B. van Leeuwen[1,2], Tessa Buckle[1,2]*, and Oscar R. Brouwer[1,2]*

[1]*Department of Urology, Netherlands Cancer Institute, Amsterdam, The Netherlands;* [2]*Interventional Molecular Imaging Laboratory, Department of Radiology, Leiden University Medical Centre, Leiden, The Netherlands;* [3]*Department of Pathology, Netherlands Cancer Institute, Amsterdam, The Netherlands; and* [4]*Department of Head and Neck Surgery, Netherlands Cancer Institute, Amsterdam, The Netherlands*

In penile squamous cell carcinoma (pSCC), primary surgery aims to obtain oncologically safe margins while minimizing mutilation. Surgical guidance provided by receptor-specific tracers could potentially improve margin detection and reduce unnecessary excision of healthy tissue. Here, we present the first results of a prospective feasibility study for real-time intraoperative visualization of pSCC using a fluorescent mesenchymal–epithelial transition factor (c-MET) receptor targeting tracer (EMI-137). **Methods:** EMI-137 tracer performance was initially assessed ex vivo ($n = 10$) via incubation of freshly excised pSCC in a solution containing EMI-137 (500 nM). The in vivo potential of c-MET targeting and intraoperative tumor visualization was assessed after intravenous administration of EMI-137 to 5 pSCC patients scheduled for surgical resection using a cyanine-5 fluorescence camera. Fluorescence imaging results were related to standard pathologic tumor evaluation and c-MET immunohistochemistry. Three of the 5 in vivo patients also underwent a sentinel node resection after local administration of the hybrid tracer indocyanine green–^{99m}Tc-nanocolloid, which could be imaged using a near-infrared fluorescence camera. **Results:** No tracer-related adverse events were encountered. Both ex vivo and in vivo, EMI-137 enabled c-MET–based tumor visualization in all patients. Histopathologic analyses showed that all pSCCs expressed c-MET, with expression levels of at least 70% in 14 of 15 patients. Moreover, the highest c-MET expression levels were seen on the outside rim of the tumors, and a visual correlation was found between c-MET expression and fluorescence signal intensity. No complications were encountered when combining primary tumor targeting with lymphatic mapping. As such, simultaneous use of cyanine-5 and indocyanine green in the same patient proved to be feasible. **Conclusion:** Fluorescence imaging of c-MET receptor–expressing pSCC tumors after intravenous injection of EMI-137 was shown to be feasible and can be combined with fluorescence-based lymphatic mapping. This combination is unique and paves the way toward further development of this surgical guidance approach.

Key Words: penile squamous cell carcinoma; fluorescence-guided surgery; c-MET receptor; receptor-targeted imaging; sentinel node; multicolor

J Nucl Med 2022; 63:51–56
DOI: 10.2967/jnumed.120.261864

Surgical resection remains the mainstay of treatment for primary penile squamous cell carcinoma (pSCC). The potential morbidity of surgery, and the impact on the patient's sexuality and quality of life, can be minimized by performing penile-sparing surgery in early disease (*1*). Unfortunately, in today's practice, positive margins—potentially causing local cancer recurrence—still occur in up to 36% of patients (*2*). Hence, penile-sparing surgery needs to strike an optimal balance between acquiring oncologically safe resection margins and maximizing residual function and appearance.

Penile cancer surgery is one of the common indications in which image-guided sentinel node resections are applied as routine care (*3*). The current state of the art relies on lymphatic migration of the near-infrared tracer indocyanine green (ICG)–^{99m}Tc-nanocolloid after local administration (Fig. 1) (*3*).

Expression of the c-MET oncogene has been recorded in up to 87% of pSCC patients (*4*). Previously, it was shown that use of the far-red (cyanine-5 [Cy5]) fluorescent mesenchymal–epithelial transition factor (c-MET)–targeting peptide EMI-137 (formally known as GE-137), in combination with experimental cameras, was able to facilitate receptor-mediated fluorescence-guided resection of c-MET–positive lesions during colonoscopy (0.13 mg/kg) and esophagoscopy (0.09–0.13 mg/kg) (*5*–*7*) after intravenous tracer administration (Fig. 1).

Recent efforts have shown that commercial fluorescence cameras can be modified slightly to allow for Cy5 imaging and can even be used for multicolor imaging applications that allow visualization of 2 complementary tracers in the same patient (*8*,*9*).

In this feasibility study in pSCC patients, we evaluated whether ex vivo incubation could predict the in vivo success of c-MET receptor–targeted fluorescence-guided imaging and whether this technology could be applied simultaneously with fluorescence-guided lymphatic mapping (Fig. 1).

MATERIALS AND METHODS

Patients

Fifteen patients with clinical suspicion of pSCC were prospectively included for either ex vivo ($n = 10$) or in vivo ($n = 5$) evaluation.

Received Dec. 21, 2020; revision accepted Apr. 20, 2021.
For correspondence or reprints, contact Oscar R. Brouwer (o.brouwer@nki.nl) or Tessa Buckle (T.Buckle@lumc.nl).
*Contributed equally to this work.
Published online May 14, 2021.

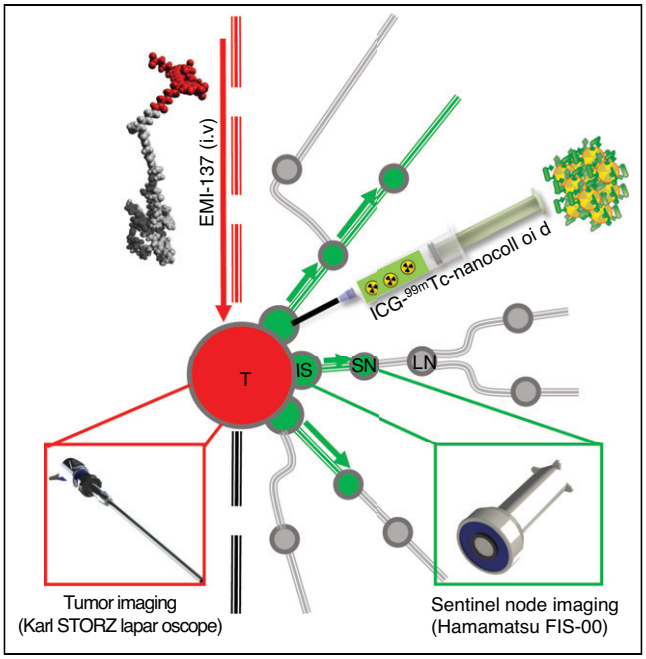

FIGURE 1. Logistics of hybrid and multicolor imaging in penile cancer patients. (Right) Local administration of hybrid tracer ICG–^{99m}Tc-nanocolloid (sentinel node imaging; peak excitation wavelength = 800 nm; peak emission wavelength = 820 nm) is followed by sentinel node identification based on planar lymphoscintigraphy and SPECT/CT at 15 min and 2 h. During surgical procedure (4–24 h after tracer administration), preoperative images serve as personalized surgical roadmap for intraoperative radio- and fluorescence-guided sentinel node localization. ICG-based fluorescence guidance was achieved using PDE-FIS from Hamamatsu Photonics (*3*). (Left) Fluorescence-guided tumor visualization was achieved at 3 h after intravenous administration of Cy5-fluorescent C-Met targeting tracer EMI-137 (peak excitation wavelength, 640 nm; peak emission wavelength, 680 nm). Intraoperative imaging was achieved through (first-in-humans) use of clinical-grade Cy5-dedicated laparoscope from Karl Storz Endoskope (*11*). IS = injection site; i.v. = intravenous; LN = lymph node; SN = sentinel node; T = tumor.

Patient and tumor characteristics are presented in Table 1. For in vivo assessment of EMI-137 (Edinburgh Molecular Imaging), patients with severe kidney insufficiency and patients who actively planned pregnancy of their partners or abstained from using 2 forms of barrier contraceptives were excluded. Three of the 5 in vivo patients also underwent sentinel node resection for expected T1G2 or higher disease with clinically nonsuggestive lymph nodes. Pathologic TNM stage, primary tumor surgery type, differentiation grade, lymphovascular invasion, perineural growth, presence of penile intraepithelial neoplasia, radicality, margin size, tumor diameter, infiltration depth, and p16 status were recorded (Table 1). The institutional review board approved the ex vivo study, and the medical ethical committee approved the in vivo study. All subjects signed an informed consent form. The in vivo study was registered in the European Clinical Trials Register (2019-003022-24).

Tracer Preparation

For ex vivo sample assessment, EMI-137 was dissolved in phosphate-buffered saline to a concentration of 500 nM (20 mL per sample). For in vivo use, EMI-137 was prepared for intravenous administration under good manufacturing practices by our institutions' pharmacy. To this end, the content of a vial of EMI-137 was reconstituted with 5.0 mL of sterile water, after which the vial contained an isotonic 4.8 mg/mL solution of EMI-137 in a 50 nM phosphate buffer. On the morning of surgery, the pharmacy department prepared a syringe with the exact EMI-137 dose based on patient weight. Additional details on the fluorescent EMI-137 tracer and an in-depth description of its pharmacokinetics were previously published by Burggraaf et al. (*5*).

ICG–^{99m}Tc-nanocolloid was prepared according to previously described methods (*3*,*10*).

Fluorescence Imaging Modalities

White-light and far-red fluorescence imaging were conducted using a clinical-grade Cy5 fluorescence camera (Karl Storz Endoskope GmbH; (*11*)) complemented with in-house–developed image-processing software that allowed color coding of the fluorescence signal for improved visualization and distinction of intensity differences, allowing direct correlation to the tumor-to-background ratio (TBR; the ratio between relative fluorescence units (*12*) in the tumor and in the surrounding tissue). This image-processing software was built to run in real time and was written in the C++ programming language. To map differences in fluorescence intensity measured to different color values, open-source computer vision libraries (OpenCV) were used. The color map allowed real-time visualization of the fluorescence signal's distribution within the tissue sample (pseudocolored fluorescence overlay visible on a separate screen) and representation of the TBR via an intensity-based scale bar (fluorescence signal intensity differences represented via a color spectrum). The TBRs were confirmed using ImageJ software by dividing the fluorescent signal intensity in the tumor by the fluorescent signal intensity in background tissue.

Near-infrared fluorescence imaging was performed using a PDE-FIS (FIS-00) fluorescence camera (Hamamatsu Photonics).

Ex Vivo Assessment of Feasibility of c-MET Targeting

Resected primary tumor specimens were collected directly after excision and assessed immediately (Fig. 2A). Tumor samples were bisected in the pathology department before ex vivo imaging. For ex vivo assessment of in vivo targeting feasibility, samples were incubated in a solution containing EMI-137 (500 nM, 20 mL) for 5 min. The samples were then rinsed twice with phosphate-buffered saline to clear unbound EMI-137. Samples obtained from patients who received EMI-137 via intravenous administration were imaged without further pretreatment.

In Vivo Tracer Administration and Fluorescence-Guided Imaging

Five pSCC patients received intravenous administration of EMI-137 (0.13 mg/kg; (*5*)) at 3 h (±30 min) before surgery. Adverse events were registered up to 2 wk after intravenous tracer injection. Three patients also underwent a sentinel node resection based on the local intradermal administration of ICG–^{99m}Tc-nanocolloid in 3 depots and preoperative nodal identification (lymphoscintigraphy and SPECT/CT imaging at 15 min and 2 h after tracer administration (Fig. 1) (*3*,*10*).

To maintain the standard surgical procedure until the ability of EMI-137 to reliably visualize tumor tissue was demonstrated, the operating surgeon was not aware of the intraoperative far-red fluorescence imaging results. The surgical assistant performed Cy5-based imaging. White-light and fluorescence images of the tumor were obtained in the operation room immediately before incision, as well as intra- and postoperatively. Resection of sentinel nodes was based on their anatomic location on SPECT/CT, intraoperative radio guidance (with a γ-probe), and near-infrared fluorescence guidance. Excised samples were also imaged ex vivo.

Pathologic Assessment

After ex vivo imaging, samples were formalin-fixed and paraffin-embedded. Three-micrometer sections were subjected to either c-MET or hematoxylin and eosin staining. Immunohistochemistry of the

TABLE 1
Characteristics of All 15 Ex Vivo and In Vivo Patients

Parameter	Injection to surgery (min)	cT	cN	cM	Surgery	pT	pN	pGr	PeIN	LVI	PNI	R	Diameter (mm)	Infiltration depth (mm)	p16	c-MET expression (%)	c-MET score	TBR
Ex vivo		2	1	0	Partial penectomy	3	1	2	No	Yes	Yes	Yes	28	24	Pos	70	0.7	3.2
Ex vivo		2	0	x	Recircumcision	1a	0	2	Yes	No	No	Yes	5	2	Neg	95	0.85	2
Ex vivo		2	0	x	Partial penectomy	1a	0	1	Yes	No	No	Yes	9	2	Neg	90	1.35	2.8
Ex vivo		2	0	x	Local excision with circumcision	1a	0	2	Yes	No	No	Yes	25	3	Neg	90	0.9	2.5
Ex vivo		2	2	0	Local excision with circumcision	1a	x	2	No	No	—	Yes	48	17	Neg	70	1.5	2.2
Ex vivo		3	0	x	Subtotal penectomy	3	x	3	No	Yes	Yes	No	52	—	Neg	90	0.9	2.6
Ex vivo		2	0	x	Local excision with circumcision	1a	0	2	No	No	No	Yes	43	5	Pos	80	1.1	3.4
Ex vivo		3	3	0	Partial penectomy	3	3	2	No	Yes	—	Yes	33	24	Pos	100	2.3	2.9
Ex vivo		2	0	x	Partial penectomy	3	0	3	Yes	Yes	Yes	Yes	21	14	Pos	95	1.65	2.3
Ex vivo		2	0	x	Partial penectomy	2	0	2	No	Yes	Yes	Yes	55	—	Neg	95	1.2	2.7
In vivo	263	1	0	x	Local excision	1a	x	1	Yes	No	—	Yes	18	0,5	—	80	1.1	2.1
In vivo	236	2	3	1	Partial penectomy	3	x	3	Yes	Yes	No	Yes	21	—	Pos	100	1.75	4.2
In vivo	245	2	0	x	Local excision and circumcision	1a	0	2	No	No	No	Yes	18	4,5	Neg	30	0.4	2.1
In vivo	202	2	0	x	Local excision and circumcision	1a	0	2	No	No	No	Yes	12	2	Pos	100	2.3	2
In vivo	183	1	0	x	Partial glansectomy	1a	0	2	No	No	Yes	Yes	13	6	Neg	90	1.55	3.3

pGr = pathologic differentiation grade; PeIN = penile intraepithelial neoplasia; LVI = lymphovascular invasion; PNI = perineural invasion; R = radicality; pos = positive; neg = negative; x = not staged; — = not reported.

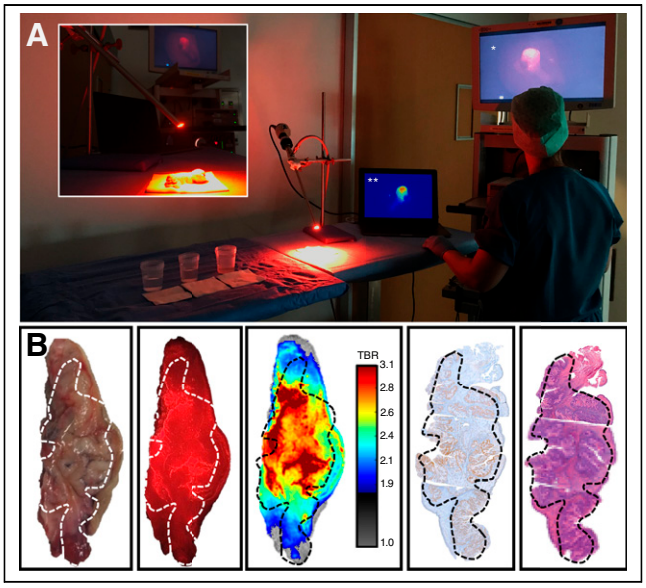

FIGURE 2. Ex vivo c-MET–targeted imaging in penile cancer.(A) For ex vivo assessment of targeting feasibility, pSCC tissue samples obtained after surgical tumor excision in penile cancer patients were incubated in solution containing EMI-137 (5 min, including 2 washing steps, shown on left). Imaging was performed using Karl Storz Endoskope Cy5 laparoscope; results were depicted on 2 screens showing unprocessed (*) and real-time processed (**) fluorescence image. Inset shows detailed view of illumination of tissue sample. (B) From left to right: white-light image of excised tissue sample; ex vivo Cy5-based fluorescence imaging of incubated tissue (fluorescence in red); real-time image processing of fluorescence signal (heat-map color coding); c-MET immunohistochemistry; and hematoxylin and eosin staining of tissue samples. Tumor delineation (dashed line) was based on hematoxylin and eosin staining.

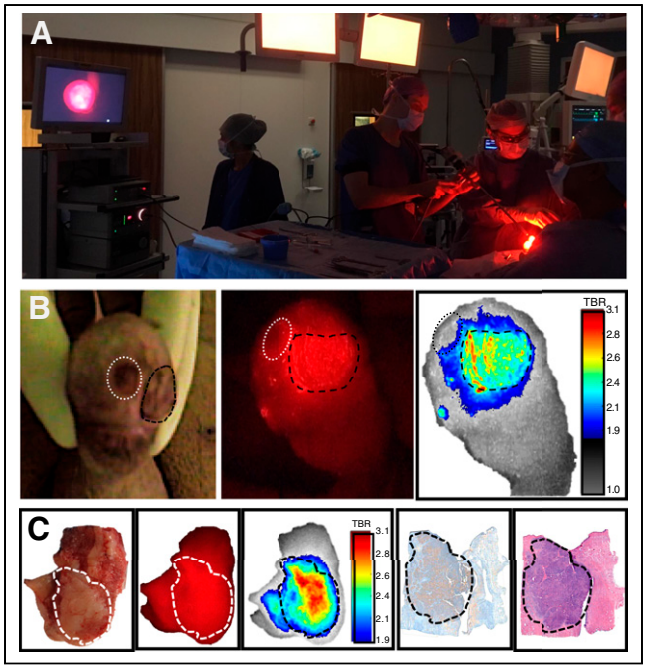

FIGURE 3. Tumor imaging. (A) Overview of surgical set-up within operating room. (B) From left to right: preincision imaging of penis showing both urethral orifice (urinary meatus) and tumor; Cy5-based localization of tumor; and real-time color coding of fluorescence signal (with color-coded scale bar representing TBR). Tumor is encircled in black, and dotted white line indicates ulcus after biopsy, which found—at pathologic examination—penile intraepithelial neoplasia. (C) From left to right: ex vivo imaging of excised tumor specimen; Cy5-based fluorescence image; real-time image processing of fluorescence signal (heat-map color coding); c-MET immunohistochemistry; and hematoxylin and eosin staining of tissue samples. Tumor delineation (dashed line) was based on hematoxylin and eosin staining.

formalin-fixed, paraffin-embedded tumor samples was performed on a BenchMark Ultra autostainer (Ventana Medical Systems). Briefly, paraffin sections 3 μm thick were cut, heated at 75°C for 28 min, and deparaffinized in the instrument with EZ Prep solution (Ventana Medical Systems). Heat-induced antigen retrieval was performed using Cell Conditioning 1 (Ventana Medical Systems) for 64 min at 95°C. c-MET was detected using clone SP44 (ready to use, 16 min at 360°C; Roche Diagnostics). Bound c-MET was detected using the UltraView Universal 3,3-diaminobenzidine detection kit (Ventana Medical Systems). Slides were counterstained with hematoxylin and bluing reagent (Ventana Medical Systems).

A dedicated urologic cancer pathologist scored stained sections. Percentages of positive cells were scored for 4 staining intensity categories (−, +, ++, and +++). From this, a c-MET score was calculated by multiplying the percentage of positive tumor area by the intensity of the staining (1 [+] × % positive + 2 [++] × % positive + 3 [+++] × % positive) (*13*). In short, a c-MET score is the average expression intensity of the complete tumor area. The possible c-MET scores range from 0 (no expression at all) to 3 (100% +++ expression) (*13*).

Excised lymph nodes were pathologically examined for the presence of macro- or micrometastases or isolated tumor cells, according to previously described protocols (*3*). The resected penectomy specimens were examined and classified for pathologic tumor stage and grade (*14*).

Statistical Analysis

For continuous variables, the range is reported. The Mann–Whitney *U* test was used to compare TBR between ex vivo and in vivo samples. Spearman correlation was used for comparison of continuous variables. A *P* value of less than 0.05 was deemed significant.

RESULTS

Initial ex vivo assessment of the feasibility of tumor visualization based on c-MET targeting (Fig. 2) resulted in tumor identification in all 10 tumor specimens. TBRs were in the range of 2.0 ± 0.6 to 3.4 ± 0.3 (Table 1). The identification of tumor tissue was improved by the real-time conversion of the fluorescence output to a heat-map–based color coding (Fig. 2B). Immunohistochemistry confirmed c-MET expression in all tumors and showed the highest c-MET expression at the edge of the tumor (Fig. 2B). Membranous c-MET expression was seen in 70%–100% of cells per specimen (median, 90%), providing c-MET scores in the range of 0.7–2.3 (median, 1.2) (*13*). Standard pathologic processing was not affected by the presence of Cy5 fluorescence in the surgical sample.

Based on the successful targeting of c-MET in ex vivo surgical specimens, EMI-137 was intravenously administered to 5 patients with pSCC (Fig. 3). Far-red fluorescence imaging allowed identification of the primary tumor (Fig. 3B). Again, color coding obtained after (real-time) image processing provided increased discrimination between the tumor and the surrounding healthy tissue. No interference of renally cleared EMI-137 was observed (Fig. 3B). TBRs after intravenous tracer administration were

similar to those reported for the ex vivo incubation, namely between 2.0 ± 0.4 and 4.2 ± 0.9 (Table 1; $P = 0.68$).

In the 3 patients who also underwent sentinel node biopsy, preoperatively identified sentinel nodes (Figs. 4A–4C) were removed using a combination of radio guidance and fluorescence guidance. Fluorescence imaging prior to resection of the sentinel node enabled visualization of both lymphatic drainage from the injection site (Fig. 4D) and superficially located sentinel nodes (Fig. 4D). The signal intensity increased when the incision was placed and overlying tissue was resected. All 11 resected sentinel nodes were tumor-negative at pathology. This was underlined by the presence of a clear ICG-related signal in the sentinel node, whereas no clear tumor-related Cy5 signal could be detected (Fig. 4E). Moreover, whereas the injection site for ICG–^{99m}Tc-nanocolloid and the location of the tumor were within the same field of view (Fig. 1), near-infrared fluorescence guidance was shown not to be impaired by the presence of far-red fluorescence, or vice versa (Figs. 3B, 4D, and 4E).

Histopathologically, membranous c-MET expression was seen in all tumors (range, 30%–100%; median, 95%), with expression of at least 70% of cells per excised specimen in 4 of 5 tumors, resulting in c-MET scores in the range of 0.4–2.3 (median, 1.7; Table 1). Comparative to the ex vivo specimens, c-MET expression was present throughout the tumor, but the expression was increased at the tumor edge (Fig. 3C).

A (nonsignificant) trend of rising TBR with an increasing c-MET score was observed (Spearman correlation coefficient, 0.203; $P = 0.469$). Interestingly, the c-MET score and TBR appeared to be higher in patients with LVI, a T stage of at least 2, cN+, and p16 positivity (Table 1), which may support the hypothesis that patients with a worse tumor stage or human papillomavirus–induced tumors might especially benefit from c-MET–targeted surgery.

DISCUSSION

In this pilot study on penile cancer patients, we found that EMI-137, a c-MET–specific fluorescent tracer, enabled receptor-mediated ex vivo and in vivo fluorescence-based visualization of primary pSCC (TBR > 2; Table 1). In line with previous literature, no adverse events were recorded after intravenous administration of EMI-137 (*5*). Furthermore, Cy5-based far-red imaging proved to be compatible with near-infrared fluorescence imaging (ICG–^{99m}Tc-nanocolloid) performed during the same procedure.

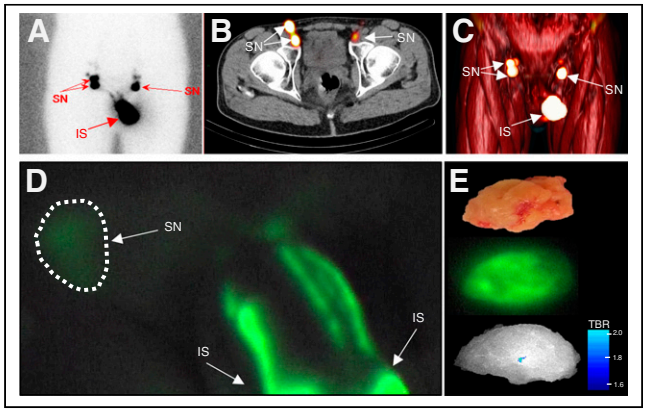

FIGURE 4. Sentinel node imaging. (A) Standard lymphography after local administration of ICG–^{99m}Tc-nanocolloid specifying sentinel nodes. (B and C) Accompanying SPECT/CT image (B) and 3D representation of SPECT/CT results (C), placing sentinel nodes in their anatomic context. (D) Preincision ICG-based fluorescence image showing injection site of ICG–^{99m}Tc-nanocolloid with drainage through lymphatics toward sentinel node (encircled). (E) Postexcision white-light image of sentinel node (top), with ICG image (center) and infrared image after image processing (bottom, including color-coded scale bar for TBR). IS = injection site; SN = sentinel node.

The finding that all pSCC tumors expressed or overexpressed c-MET by at least 70% with preselection of patients and that the tumor tissue could be stained using EMI-137 suggests that c-MET is a potential target for image guidance for pSCC. By masking the surgeon from the far-red fluorescence imaging result during surgery, the standard surgical procedure remained unaffected, and no decisions that could alter patient treatment were made before the assessment of the feasibility of the c-MET targeting approach. However, this approach also enabled the possibility of intraoperative margin assessment. Nevertheless, postoperative assessment underlined the presence of c-MET expression in all samples and that the c-MET–related fluorescence signal was visible at the edge of all tumors (Figs. 2 and 3), indicating possible future potential in this cancer type. The plurality of fluorescent tracers currently being evaluated in clinical studies for a variety of tumor types (e.g., pancreatic cancer, head and neck cancer, and melanoma) also paves the way for the assessment of other possible imaging targets and targeted tracers for penile cancer (*15–21*).

Our study confirmed the high c-MET expression rate of 87% in pSCC found by Gunia et al. (*4*). In all 15 patients, far-red fluorescence could be related to the presence of the c-MET receptor at immunohistochemistry. These results are in line with c-MET–specific fluorescent tracer reports from studies on Barrett esophagus and dysplastic colorectal polyps (*5–7*). This correlation and high expression pattern make the c-MET receptor potentially a promising target for tumor-specific applications in pSCC. Further investigation in a larger patient cohort will be required to substantiate the correlation between c-MET score and TBR, to investigate the ability to reduce positive surgical margins, and to identify the patient group that will benefit most from c-MET–based fluorescence-guided surgery.

This study also showed that primary tumor imaging of far-red (Cy5) fluorescence (peak excitation wavelength, 640 nm; peak emission wavelength, 680 nm) using a first-in-humans laparoscopic camera from Karl Storz Endoskope could be performed alongside near-infrared (ICG) imaging of ICG–^{99m}Tc-nanocolloid (peak excitation wavelength, 800 nm; peak emission wavelength, 820 nm) using a clinical-grade fluorescence camera. Fortunately for the patients, the evaluated lymph nodes in this study did not contain metastases, and no Cy5-related signal could be detected in these nodes. Although the utility of targeted tracers for visualization of micrometastases can be debated (*22*), tumor-targeted far-red imaging has been shown to allow sentinel node mapping successfully (*20*). The combined use of 2 different fluorescent entities within the same procedure supports the future exploration of multicolor fluorescence-guided surgery avenues (*9*) that allow visualization of distinct anatomic features (e.g., tumor and sentinel nodes) alongside each other.

CONCLUSION

The results from this pilot study suggest that c-MET is a promising target for fluorescence-guided tumor identification, with the potential to improve margin assessment in pSCC. The c-MET–targeted approach proved to be compatible with lymphatic mapping

performed on the same patient using multicolor fluorescence guidance based on both far-red (Cy5) and near-infrared (ICG) imaging.

DISCLOSURE

This research was financially supported by a Netherlands Organization for Scientific Research TTW-VICI grant (grant TTW 16141). EMI-137 was provided by Edinburgh Molecular Imaging (EMI), Karl Storz Endoskope provided the Cy5 fluorescence camera, and the FIS-00 near-infrared fluorescence camera was made available by Hamamatsu Photonics. No other potential conflict of interest relevant to this article was reported.

ACKNOWLEDGMENTS

We thank Alwin Huitema, Erik van Muilekom, Jeroen Visser, Eva Offringa, Florian van Beurden, Nina Heimburger, Danny van Willigen, Fabian van Hensbergen, Krijn Houwing, and Leon Slof for assistance with the set-up, logistics, conduction, chemistry, and software of this study. We also acknowledge the NKI-AVL Core Facility Molecular Pathology & Biobanking (CFMPB) for lab support.

KEY POINTS

QUESTION: Is the c-MET specific tracer EMI-137 feasible for intraoperative visualization of pSCC?

PERTINENT FINDING: This observational fluorescent tracer study describes findings on ten fresh *ex vivo* tumour specimens and five patients who were intravenously injected with a c-MET specific fluorescent tracer. All tumours were visible via fluorescence imaging, and all expressed c-MET on immunohistochemistry. Thus, c-MET fluorescent imaging appears to be feasible in pSCC. Moreover, this c-MET targeted approach proved to be compatible with lymphatic mapping performed in the same patient.

IMPLICATIONS FOR PATIENT CARE: This study indicates that during future pSCC surgery, fluorescent primary tumour visualization is feasible, even in combination with sentinel node procedures. With targeted tracers like EMI-137 and multicolor imaging capabilities, technical capabilities of providing image guidance toward the primary tumour are now emerging.

REFERENCES

1. Kieffer JM, Djajadiningrat RS, van Muilekom EAM, Graafland NM, Horenblas S, Aaronson NK. Quality of life for patients treated for penile cancer. *J Urol.* 2014; 192:1105–1110.
2. Baumgarten A, Chipollini J, Yan S, et al. Penile sparing surgery for penile cancer: a multicenter international retrospective cohort. *J Urol.* 2018;199:1233–1237.
3. Dell'Oglio P, de Vries HM, Mazzone E, et al. Hybrid indocyanine green–^{99m}Tc-nanocolloid for single-photon emission computed tomography and combined radio- and fluorescence-guided sentinel node biopsy in penile cancer: results of 740 inguinal basins assessed at a single institution. *Eur Urol.* 2020;78:865–872.
4. Gunia S, Erbersdobler A, Hakenberg OW, Koch S, May M. C-MET is expressed in the majority of penile squamous cell carcinomas and correlates with polysomy-7 but is not associated with MET oncogene amplification, pertinent histopathologic parameters, or with cancer-specific survival. *Pathol Res Pract.* 2013;209:215–220.
5. Burggraaf J, Kamerling IMC, Gordon PB, et al. Detection of colorectal polyps in humans using an intravenously administered fluorescent peptide targeted against c-Met. *Nat Med.* 2015;21:955–961.
6. de Jongh SJ, Voskuil FJ, Schmidt I, et al. C-Met targeted fluorescence molecular endoscopy in Barrett's esophagus patients and identification of outcome parameters for phase-I studies. *Theranostics.* 2020;10:5357–5367.
7. de Jongh SJ, Vrouwe JPM, Voskuil FJ, et al. The optimal imaging window for dysplastic colorectal polyp detection using c-Met–targeted fluorescence molecular endoscopy. *J Nucl Med.* 2020;61:1435–1441.
8. Schottelius M, Wurzer A, Wissmiller K, et al. Synthesis and preclinical characterization of the PSMA-targeted hybrid tracer PSMA-I&F for nuclear and fluorescence imaging of prostate cancer. *J Nucl Med.* 2019;60:71–78.
9. van Beurden F, van Willigen DM, Vojnovic B, et al. Multi-wavelength fluorescence in image-guided surgery, clinical feasibility and future perspectives. *Mol Imaging.* 2020;19:1536012120962333.
10. Brouwer OR, Buckle T, Vermeeren L, et al. Comparing the hybrid fluorescent-radioactive tracer indocyanine green-^{99m}Tc-nanocolloid with ^{99m}Tc-nanocolloid for sentinel node identification: a validation study using lymphoscintigraphy and SPECT/CT. *J Nucl Med.* 2012;53:1034–1040.
11. van Willigen DM, van den Berg NS, Buckle T, et al. Multispectral fluorescence guided surgery: a feasibility study in a phantom using a clinical-grade laparoscopic camera system. *Am J Nucl Med Mol Imaging.* 2017;7:138–147.
12. Tummers WS, Warram JM, van den Berg NS, et al. Recommendations for reporting on emerging optical imaging agents to promote clinical approval. *Theranostics.* 2018;8:5336–5347.
13. Mazières J, Brugger W, Cappuzzo F, et al. Evaluation of EGFR protein expression by immunohistochemistry using H-score and the magnification rule: re-analysis of the SATURN study. *Lung Cancer.* 2013;82:231–237.
14. Hakenberg OW, Comperat E, Minhas S, Necchi A, Protzel C, Watkin N. Penile cancer. European Association of Urology website. https://uroweb.org/guideline/penile-cancer/. Accessed September 30, 2021.
15. van Leeuwen FWB, Schottelius M, Brouwer OR, et al. Trending: radioactive and fluorescent bimodal/hybrid tracers as multiplexing solutions for surgical guidance. *J Nucl Med.* 2020;61:13–19.
16. Hernot S, van Manen L, Debie P, Mieog JSD, Vahrmeijer AL. Latest developments in molecular tracers for fluorescence image-guided cancer surgery. *Lancet Oncol.* 2019;20:e354–e367.
17. Joshi BP, Wang TD. Targeted optical imaging agents in cancer: focus on clinical applications. *Contrast Media Mol Imaging.* 2018;2018:2015237.
18. van Keulen S, Nishio N, Fakurnejad S, et al. Intraoperative tumor assessment using real-time molecular imaging in head and neck cancer patients. *J Am Coll Surg.* 2019;229:560–567.e1.
19. Tummers WS, Miller SE, Teraphongphom NT, et al. Intraoperative pancreatic cancer detection using tumor-specific multimodality molecular imaging. *Ann Surg Oncol.* 2018;25:1880–1888.
20. Zanoni DK, Stambuk HE, Madajewski B, et al. Use of ultrasmall core-shell fluorescent silica nanoparticles for image-guided sentinel lymph node biopsy in head and neck melanoma. *JAMA Netw Open.* 2021;4:e211936.
21. Nishio N, van den Berg NS, van Keulen S, et al. Optical molecular imaging can differentiate metastatic from benign lymph nodes in head and neck cancer. *Nat Commun.* 2019;10:5044.
22. van Leeuwen FWB, Winter A, van Der Poel HG, et al. Technologies for image-guided surgery for managing lymphatic metastases in prostate cancer. *Nat Rev Urol.* 2019;16:159–171.